Cost effective accurate coarse-grid method for highly convective multidimensional unsteady flow

Article · December 1990

CITATIONS
11

READS
64

2 authors:

Brian Phillip Leonard
University of Akron
74 PUBLICATIONS **6,979** CITATIONS
SEE PROFILE

Hassan Niknafs
Khazar University
10 PUBLICATIONS **83** CITATIONS
SEE PROFILE

COST-EFFECTIVE ACCURATE COARSE-GRID METHOD FOR HIGHLY CONVECTIVE MULTIDIMENSIONAL UNSTEADY FLOWS

B. P. Leonard and H. S. Niknafs
The University of Akron
Akron, OH 44325

ABSTRACT

A fundamentally multidimensional convection scheme is described based on vector transient interpolation modelling rewritten in conservative control-volume form. Vector third-order upwinding is used as the basis of the algorithm; this automatically introduces important cross-difference terms that are absent from schemes using component-wise one-dimensional formulas. Third-order phase accuracy is good; this is important for coarse-grid large-eddy or full simulation. Potential overshoots or undershoots are avoided by using a recently developed universal limiter. Higher order accuracy is obtained locally, where needed, by the cost-effective strategy of adaptive stencil expansion in a direction normal to each control-volume face; this is controlled by monitoring the absolute normal gradient and curvature across the face. Higher (than third) order cross-terms do not appear to be needed. Since the wider stencil is used only in isolated narrow regions (near discontinuities), extremely high (in this case, seventh) order accuracy can be achieved for little more than the cost of a globally third-order scheme.

INTRODUCTION

The authors have recently developed (reference 1) a cost-effective strategy for obtaining very high accuracy results for one-dimensional convective simulation on practical (i.e., coarse) grids. The method automatically produces tight nonoscillatory resolution of discontinuities without distorting smooth profiles or clipping very narrow extrema. All these desirable features are obtained for little more cost than that of the basic third-order upwind scheme on which the algorithm is based (reference 2). Figure 1 shows what can be achieved in one dimension. The figure shows computed points together with the exact solution for four profiles: a unit step, an isolated sine-squared wave $20\Delta x$ wide, a semi-ellipse $20\Delta x$ wide, and a narrow Gaussian ($\sigma = 1.94\Delta x$); at the time shown, the profiles have been translated by pure convection 45 mesh-widths to the right (100 time-steps at a Courant number of 0.45). This particular example is based on third-order upwinding in smooth regions with automatic adaptive stencil expansion to seventh- or ninth-order upwinding locally, as needed, determined by monitoring the local absolute gradient across face $(i + \frac{1}{2})$, say,

$$\text{GRAD} = |\phi_{i+1} - \phi_i| \tag{1}$$

and the corresponding local absolute average curvature

$$\text{CURVAV} = 0.5\,|(\phi_{i+2} - \phi_{i+1}) - (\phi_i - \phi_{i-1})| \tag{2}$$

The algorithm also includes an automatic discriminator which decides when to apply the universal limiter (described in reference 3) and when to relax the limiter constraints. Ideally, the discriminator should activate the limiter in order to suppress unphysical numerical oscillations which would otherwise occur near sudden changes in gradient – each side of the step and at the "feet" of the semi-ellipse – without concomitant loss of resolution of the physical extrema (especially the narrow peak of the Gaussian profile). Clearly from Figure 1, this has been achieved; simulation of the sine-squared and Gaussian profiles is essentially exact, whereas resolution of the large-gradient regions of the other profiles is very tight.

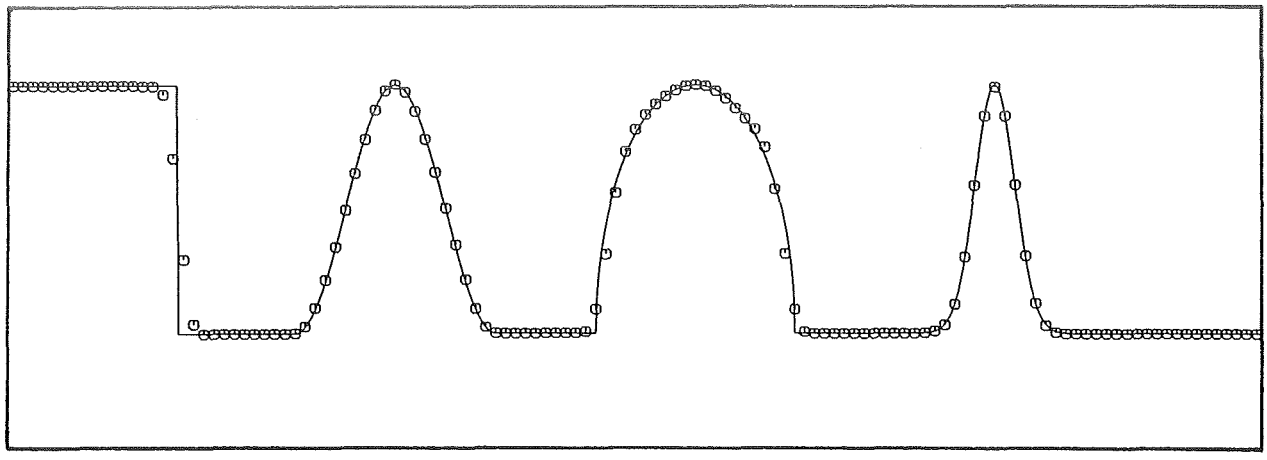

Figure 1. One-dimensional pure convection of four profiles using the cost-effective 3/7/9th-order scheme described in reference 1.

The main purpose of the present paper is to show how to extend these desirable features to multidimensional flow problems. As is well known, one-dimensional algorithms do not automatically generalize to two and three dimensions simply by using the one-dimensional scheme component-wise in each direction. However, by using the concept of vector transient interpolation modelling

$$\phi(\mathbf{x}, t + \Delta t) = \phi(\mathbf{x} - \mathbf{v}\Delta t, t) \tag{3}$$

fundamentally multidimensional convection schemes can be generated with the same properties as their one-dimensional counterparts. Very high accuracy (in both space and time) can be obtained in a simple single-time-step explicit update formulation by converting time evolution into a spatial interpolation problem at the earlier time-level, as represented by Equation (3). The multidimensional algorithms will be demonstrated in two dimensions. Once this is done, it becomes clear how to extend to three dimensions. To paraphrase a well-known aerospace quotation: algorithmically, there is a giant leap between one-dimension and two, but only a small step between two and three.

In order to demonstrate the process of converting Equation (3) into conservative control-volume form, two-dimensional transient interpolation modelling will be considered for first-order upwinding, and three second-order schemes: Lax-Wendroff (reference 4), second-order upwinding and Fromm's method (reference 5). The two-dimensional extension of the QUICKEST scheme (reference 2) represents a uniformly third-order polynomial interpolation algorithm (UTOPIA). As with QUICKEST in one dimension, UTOPIA is susceptible to unphysical overshoots and undershoots if sudden changes in gradient are involved. Essentially nonoscillatory results can be obtained by applying the universal limiter of reference 3 to the individual control-volume fluxes. Although UTOPIA has excellent phase accuracy, short-wavelength resolution is, of course, limited to third order. In principle, arbitrarily higher order resolution can be obtained locally – as in the one-dimensional scheme demonstrated in Figure 1 – by local adaptive stencil expansion. It appears that stencil expansion in a direction normal to a particular control-volume face is much more effective than expansion in the transverse direction. Thus, although transverse terms are included to third order, higher order stencil expansion is taken only in the normal direction. Results for a third/seventh-order scheme are given for the well-known rotating-velocity-field benchmark test problem using three test profiles: a cylinder, a cone, and a narrow Gaussian. In the results given here, an *ad hoc* discriminator is used in order to relax the limiter constraints near physical extrema. An automatic multidimensional discriminator is currently under development.

CONTROL-VOLUME FORMULATION

For simplicity, consider a two-dimensional square mesh (of unit grid size) with a control-volume using standard compass-point labelling. Equation (3) can be rewritten as

$$\phi_P^{n+1} = \phi(0,0,t+\Delta t) = \phi(-u\Delta t, -v\Delta t, t) = \phi^n(-u\Delta t, -v\Delta t) \tag{4}$$

where $\phi^n(x,y)$ represents the behaviour of the convected field variable in the (upstream-biassed) vicinity of the control volume. The following algorithms depend on the functional form asumed for $\phi^n(x,y)$. Assume that u and v are both positive and (for the moment) constant.

First-Order Upwinding

For example, consider the bilinear expression

$$\phi^n(x,y) = a + bx + cy + dxy \tag{5}$$

The four constants, a, b, c, and d, need to be evaluated; it is appropriate to use collocation at four nodal points with an upstream bias – in this case (u and v positive), these would be

$$\phi_P^n,\ \phi_W^n,\ \phi_S^n, \text{ and } \phi_{SW}^n \tag{6}$$

as shown in Figure 2, giving

$$\phi^n = \phi_P^n + (\phi_P^n - \phi_W^n)x + (\phi_P^n - \phi_S^n)y + [(\phi_P^n - \phi_W^n) - (\phi_S^n - \phi_{SW}^n)]xy \tag{7}$$

as can be easily checked by putting x and y equal to 0 or -1, independently. Using Equation (4), the explicit update algorithm becomes (for $u>0$ and $v>0$)

$$\phi_P^{n+1} = \phi_P^n - c_x(\phi_P^n - \phi_W^n) - c_y(\phi_P^n - \phi_S^n) + c_x c_y[(\phi_P^n - \phi_W^n) - (\phi_S^n - \phi_{SW}^n)] \tag{8}$$

where c_x and c_y are the respective component Courant numbers. Equation (8) can be written in the general conservative control-volume form

$$\phi_P^{n+1} = \phi_P^n + c_x\phi_w - c_x\phi_e + c_y\phi_s - c_y\phi_n \tag{9}$$

where the lower-case subscripts refer to face values, and

$$\phi_e(i,j) = \phi_w(i+1,j) \tag{10}$$

and

$$\phi_n(i,j) = \phi_s(i,j+1) \tag{11}$$

guaranteeing convective conservation. This is achieved by identifying the face values as

$$\phi_w = \phi_W^n - \frac{c_y}{2}(\phi_W^n - \phi_{SW}^n) \tag{12}$$

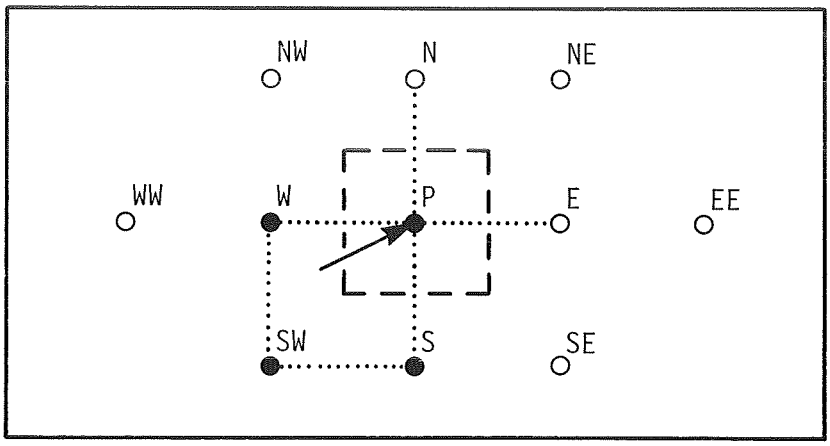

Figure 2. Compass-point notation, showing nodes involved in the first-order upwind scheme (solid dots) for $u,v>0$.

and

$$\Phi_s = \Phi_S^n - \frac{c_x}{2}(\Phi_S^n - \Phi_{SW}^n) \tag{13}$$

again for u, $v>0$, of course. Equation (12), for example, can be rewritten in a form valid for positive and negative velocities as

$$\Phi_w = \Phi_w^L - \frac{\mathrm{SGN}(c_x)}{2}\,\mathrm{GRADN} - \frac{c_y}{2}\,\mathrm{GRADT} \tag{14}$$

introducing the linearly interpolated face-value

$$\Phi_w^L = \frac{1}{2}(\Phi_P^n + \Phi_W^n) \tag{15}$$

the normal gradient across the west face

$$\mathrm{GRADN} = \Phi_P^n - \Phi_W^n \tag{16}$$

with upwind bias determined by the sign of c_x

$$\mathrm{SGN}(c_x) = \pm 1 \quad \text{for } c_x \gtrless 0 \tag{17}$$

and the upwind-biassed transverse gradient

$$\mathrm{GRADT} = \Phi_W - \Phi_{SW} \quad \text{for } c_x>0 \text{ and } c_y>0 \tag{18}$$

$$= \Phi_{NW} - \Phi_W \quad \text{for } c_x>0 \text{ and } c_y<0 \tag{19}$$

$$= \Phi_P - \Phi_S \quad \text{for } c_x<0 \text{ and } c_y>0 \tag{20}$$

$$= \Phi_N - \Phi_P \quad \text{for } c_x<0 \text{ and } c_y<0 \tag{21}$$

A similar expression can be written for ϕ_s. Then the east and north face values are obtained from Equations (10) and (11). Finally, if c_x and c_y appearing in Equation (14) (and the analogous expression for ϕ_s) are interpreted as local face values of the respective component Courant numbers, the formulas can be considered to be valid for a spatially varying convecting velocity field.

Second-Order Central

Consider the second-order expression

$$\phi^n = a + bx + cx^2 + dy + ey^2 + fxy \tag{22}$$

The six constants are determined by collocation at six nodal points: ϕ_P and the four surrounding points (ϕ_N, ϕ_S, ϕ_E, and ϕ_W) together with one additional point. As with first order, the latter point is chosen on the basis of upwind bias: ϕ_{SW} for $u>0$, $v>0$; ϕ_{NW} for $u>0$, $v<0$; ϕ_{SE} for $u<0$, $v>0$; and ϕ_{NE} for $u<0$, $v<0$. The stencil is sketched in Figure 3(a) for $u, v>0$. After evaluating the constants, using Equation (4), and rewriting in conservative control-volume form, the following formula results for the west face

$$\phi_w = \phi_w^L - \frac{c_x}{2}\,\mathrm{GRADN} - \frac{c_y}{2}\,\mathrm{GRADT} \tag{23}$$

with a similar expression for ϕ_s. As in the one-dimensional case, the difference between this and first-order upwinding, Equation (14), is the appearance of c_x itself rather than SGN(c_x) in the coefficient of the normal gradient term. Note that the transverse gradient term retains the same form.

Equation (23) is the basis of the single-time-step explicit form of the Lax-Wendroff (reference 4) or Leith (reference 6) scheme extended to two dimensions in conservative control-volume form. The first two terms on the right of Equation (23) represent the one-dimensional formula; the transverse gradient term is the significant addition for two dimensions. It should be clear that in three dimensions there would be an additional upwind-biassed transverse gradient term in the z-direction (multiplied by $-c_z/2$). The same would apply in the case of first-order upwinding.

Other Second-Order Schemes

If the stencil shown in Figure 3(b) is used to evaluate the constants in Equation (22), the two-dimensional form of second-order upwinding results. The one-dimensional form was originally discussed (in passing) by Fromm (reference 5) and was made popular in the aerospace industry by Warming and Beam (reference 7). The resulting formula (for the west face, for example) can be written

$$\phi_w = \phi_w^L - \frac{c_x}{2}\,\mathrm{GRADN} - \frac{(1-c_x)}{2}\,\mathrm{CURVN} - \frac{c_y}{2}\,\mathrm{GRADT} \tag{24}$$

where CURVN is the upwind-biassed normal curvature given by

$$\mathrm{CURVN} = \phi_P^n - 2\phi_W^n + \phi_{WW}^n \quad \text{for } c_x > 0 \tag{25}$$

or

$$\mathrm{CURVN} = \phi_E^n - 2\phi_P^n + \phi_W^n \quad \text{for } c_x < 0 \tag{26}$$

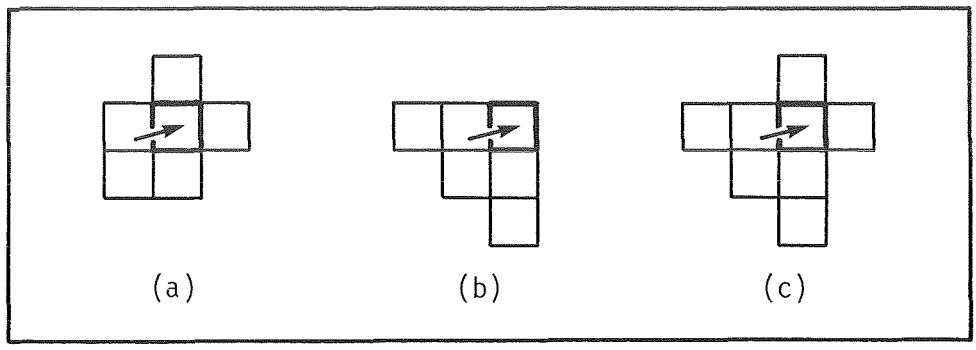

Figure 3. Second-order two-dimensional stencils ($u,v>0$). (a) Lax-Wendroff. (b) Second-order upwinding. (c) Fromm's method.

at the west face. Clearly, the appearance of the normal curvature term represents the significant difference between second-order upwinding and the second-order central formula. The same is true in one dimension. Fromm's so-called "zero-average-phase-error" method (reference 5) represents a simple average between the second-order central and second-order upwind schemes. By comparing Equations (23) and (24), it is seen that this merely reduces the CURVN coefficient by an additional factor of 2. The stencil is shown in Figure 3(c).

Third-Order Upwinding – UTOPIA

In one dimension, Fromm's method was an attempt to offset the lagging dispersion (phase error) of the Lax-Wendroff scheme by averaging it with second-order upwinding (containing inherent leading phase error). This was only partially successful; however, using the same one-dimensional stencil, it is possible to eliminate entirely the troublesome (third-derivative) dispersion term in the truncation error of the second-order schemes. The resulting explicit third-order upwind (QUICKEST) scheme has excellent phase behaviour; leading phase error stems from a small fifth-derivative term – and this is inherently damped by a fourth-derivative dissipation term (without introducing an artificial second-derivative diffusion term). The corresponding two-dimensional scheme is based on the third-order polynomial expression

$$\phi^n = a + bx + cx^2 + dx^3 + ey + fy^2 + gy^3 + hxy + ix^2y + jxy^2 \tag{27}$$

requiring 10 (upwind-biassed) collocation points. The appropriate stencil (for $u,v>0$) is sketched in Figure 4(a). The resulting formula for the west face value can then be written

$$\Phi_w = \phi_w^L - \frac{c_x}{2}\,\mathrm{GRADN} - \frac{(1-c_x^2)}{6}\,\mathrm{CURVN} - \frac{c_y}{2}\,\mathrm{GRADT} + \left(\frac{c_y^2}{6} - \frac{c_y}{4}\right)\mathrm{CURVT} + \left(\frac{c_x c_y}{3} - \frac{c_y}{4}\right)\mathrm{TWIST} \tag{28}$$

where two new terms are evident. The upwind-biassed transverse curvature is given (for the west face) by

$$\mathrm{CURVT} = \phi_{NW}^n - 2\phi_W^n + \phi_{SW}^n \quad \text{for } c_x > 0 \tag{29}$$

or

$$\mathrm{CURVT} = \phi_N^n - 2\phi_P^n + \phi_S^n \quad \text{for } c_x < 0 \tag{30}$$

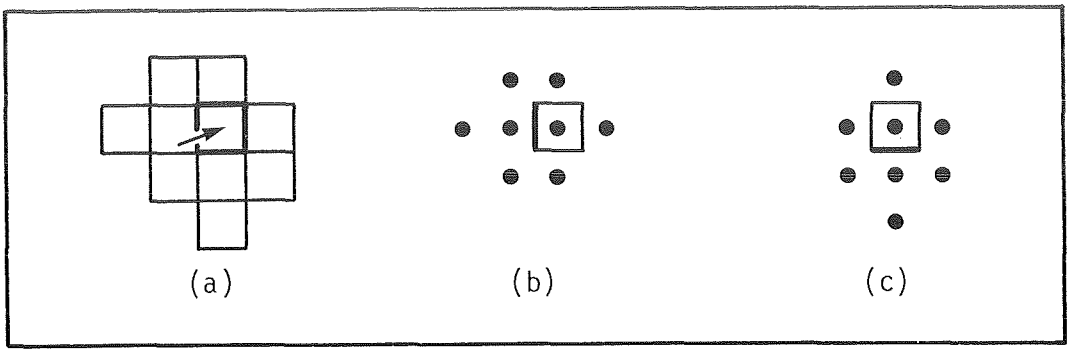

Figure 4. UTOPIA stencils. (a) Complete stencil for $u,v>0$. (b) West face stencil for arbitrary u,v. (c) South face stencil for arbitrary u,v.

The upwind-biassed "twist" term is given by

$$\text{TWIST} = (\phi_P^n - \phi_S^n) - (\phi_W^n - \phi_{SW}^n) \quad \text{for } c_y > 0 \tag{31}$$

or

$$\text{TWIST} = (\phi_N^n - \phi_P^n) - (\phi_{NW}^n - \phi_W^n) \quad \text{for } c_y < 0 \tag{32}$$

Figure 4(b) shows the stencil involved in computing the west face value when both positive and negative convecting velocity components are allowed for; Figure 4(c) shows the corresponding south face stencil. Extension to three dimensions requires additional GRADT, CURVT, and TWIST terms in an obvious manner.

UNIVERSAL LIMITER

As in the one-dimensional case, use of the two-dimensional second- and third-order schemes may result in unphysical oscillatory solutions if sharp changes in gradient are involved. In the case of the third-order scheme, this usually involves only relatively small (up to about 5%) overshoots or undershoots, at worst (reference 2). Even so, it seems desirable to eliminate this type of error (because of the possibility of nonlinear feedback instabilities in coupled equations). A universal limiting procedure, described in reference 3 for the one-dimensional case can be directly applied at each control-volume face. One first computes the multidimensional-stencil convected face value, given by Equation (28), for example. Then the "normalized" value is computed; for $c_x > 0$ at the west face, this would be

$$\tilde{\phi}_w = \frac{(\phi_w - \phi_{WW}^n)}{(\phi_P^n - \phi_{WW}^n)} \tag{33}$$

At the same time, the normalized adjacent upstream node value is computed

$$\tilde{\phi}_W = \frac{(\phi_W^n - \phi_{WW}^n)}{(\phi_P^n - \phi_{WW}^n)} \tag{34}$$

Then, if $0 \leqq \tilde{\phi}_W \leqq 1$, the normalized face value is constrained by

$$\tilde{\phi}_w \geq \tilde{\phi}_W \tag{35}$$

and

$$\tilde{\Phi}_w \leq \min(\tilde{\Phi}_W/|c_x|, 1) \tag{36}$$

Outside of the monotonic range (i.e., if $\tilde{\Phi}_W < 0$ or > 1) one could use any simple nonoscillatory scheme such as

$$\tilde{\Phi}_w = \tilde{\Phi}_W \tag{37}$$

Then the (unnormalized) face value is reconstructed using

$$\Phi_w = \Phi^n_{WW} + \tilde{\Phi}_w(\Phi^n_P - \Phi^n_{WW}) \tag{38}$$

If $c_x < 0$, the normalized west face value is given by

$$\tilde{\Phi}_w = \frac{(\Phi_w - \Phi^n_E)}{(\Phi^n_W - \Phi^n_E)} \tag{39}$$

and the normalized adjacent upstream value is then

$$\tilde{\Phi}_P = \frac{(\Phi^n_P - \Phi^n_E)}{(\Phi^n_W - \Phi^n_E)} \tag{40}$$

A similar procedure is used for the south face (based on the sign of c_y at that face). The east and north (limited) values are then given by conservation, as usual.

ADAPTIVE STENCIL EXPANSION

The uniformly third order polynomial interpolation algorithm (UTOPIA) described above is clearly limited in terms of short-wavelength resolution. In order to gain higher resolution, the same cost-effective strategy of adaptive stencil expansion – as used with such success in the one-dimensional case (reference 1) – can be used in two and three dimensions, as well. Stencil expansion in a direction normal to a particular control-volume face is fundamental for higher order resolution. Higher order transverse, twist, and other cross-terms, beyond the third-order terms of Equation (28), appear to have very little effect. Accordingly, suggested stencils for two-dimensional fifth- and seventh-order upwinding are shown in Figures 5(a) and 5(b), respectively (for $u, v > 0$). In other words, these are higher order one-dimensional schemes (reference 3) applied component-wise, together with the complete third-order cross-terms; omission of the latter terms causes severe anisotropic distortion and significant loss of accuracy in velocity fields oblique (or skew) to the grid.

Because of the (component-wise) one-dimensional nature of the proposed stencil expansion, the process can be automated by exactly the same procedure as used in the one-dimensional case. This is described in detail in reference 1. In the multidimensional code the one-dimensional adaptive stencil expansion criteria are applied independently at each of the west, south (and, in 3D, bottom) faces. In "smooth" regions, the respective values of GRAD and CURVAV are well below (pre-assigned) thresholds so that the (unlimited) UTOPIA scheme is being used. For most flows of practical interest, this will account for the overwhelming bulk of grid points, especially in three dimensions. Near isolated regions involving large values of GRAD or CURVAV at particular control-volume faces, thresholds will be exceeded, automatically switching the algorithm to fifth or seventh (or, in principle, arbitrarily higher) order at those particular points.

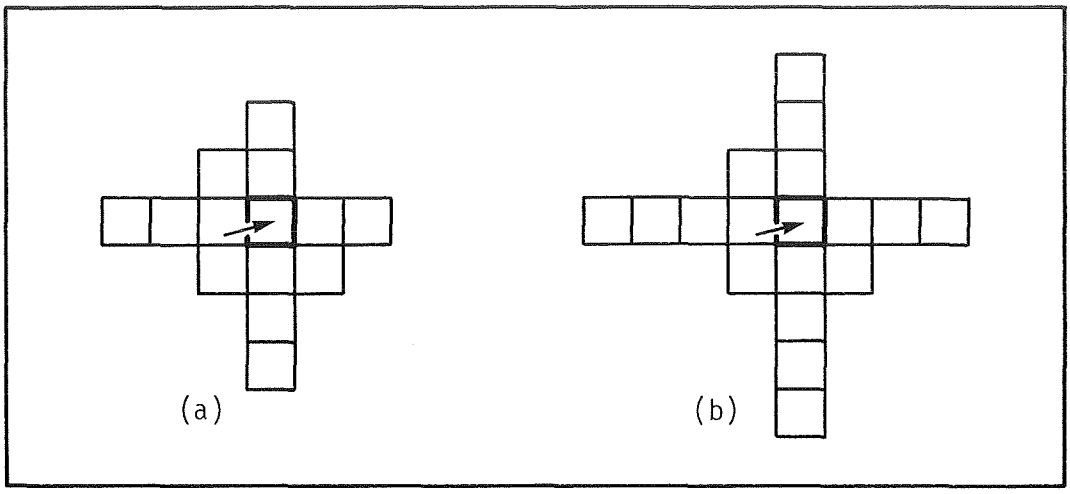

Figure 5. Stencil expansion (for $u,v>0$) from fully third-order upwind to (a) quasi-fifth-order upwind; (b) quasi-seventh-order upwind.

Two things should be noted. First, the higher order stencils will be needed only in very narrow regions (by definition of sharp change in value or gradient), thus requiring the more expensive computation at a relatively small number of grid points. This is an extremely cost-effective way to achieve very high accuracy on practical (i.e., coarse) grids – obviously an important consideration for three-dimensional simulation. Secondly, it should be clear that the location of the higher order stencils automatically changes as the flow evolves. As in the one-dimensional simulations described in reference 1, phase-accuracy is therey extremely tight. This is a critical attribute for any code designed to be used in large-eddy or full Navier-Stokes simulations.

G-EXPANSION TECHNIQUE

It is an instructive exercise to make a Fourier-von Neumann analysis (reference 8) of the multidimensional formulas discussed above and to compare Taylor expansions of their complex amplitude ratio (sometimes called "amplification factor"), G, with that of the exact solution (for constant v). This also gives some indication of how to incorporate higher order diffusion terms. For example, consider the exact complex amplitude ratio (reference 9) for the two-dimensional constant-coefficient convection-diffusion equation

$$G = \exp[-\alpha(\theta_x^2 + \theta_y^2)] \exp[-i(c_x\theta_x + c_y\theta_y)] \tag{41}$$

where α is the nondimensional diffusion parameter and the θ's are nondimensional wave-number components. A Taylor expansion of Equation (41) gives

$$G = 1 - \alpha(\theta_x^2 + \theta_y^2) - \frac{(c_x\theta_x + c_y\theta_y)^2}{2} + \frac{(c_x\theta_x + c_y\theta_y)^4}{24}$$

$$+ \frac{(c_x\theta_x + c_y\theta_y)^2\alpha(\theta_x^2 + \theta_y^2)}{2} + \frac{\alpha^2(\theta_x^2 + \theta_y^2)^2}{2} + \ldots$$

(continued)...

$$-i(c_x\theta_x + c_y\theta_y)\left\{1 - a(\theta_x^2 + \theta_y^2) - \frac{(c_x\theta_x + c_y\theta_y)^2}{6} + \frac{(c_x\theta_x + c_y\theta_y)^4}{120} + \frac{(c_x\theta_x + c_y\theta_y)^2 a(\theta_x^2 + \theta_y^2)}{6} + \frac{a^2(\theta_x^2 + \theta_y^2)^2}{2} + \ldots\right\} \tag{42}$$

At second order, note the appearance of the cross-term, $c_x\theta_x c_y\theta_y$. This is accounted for by the GRADT term in the two-dimensional second-order formulas. Component-wise application of one-dimensional second-order algorithms would miss this important term. Similarly, the cross-terms in the UTOPIA scheme are responsible for matching *all* convection terms in Equation (42) through third order in θ_x and θ_y. It is a relatively simple matter to match diffusion terms to this order, as well, building on experience with the one-dimensional QUICKEST scheme developed in reference 2 and more fully explored in reference 10. In this case, the west face value, for example becomes

$$\Phi_w = \phi_w^L - \frac{c_x}{2}\,\mathrm{GRADN} - \left[\frac{(1-c_x^2)}{6} - \frac{a_x}{2}\right]\mathrm{CURVN} - \frac{c_y}{2}\,\mathrm{GRADT} + \left(\frac{c_y^2}{6} - \frac{c_y}{4} + \frac{a_y}{2}\right)\mathrm{CURVT} + \left(\frac{c_x c_y}{3} - \frac{c_y}{4}\right)\mathrm{TWIST} \tag{43}$$

which should be compared with the pure-convection formula, Equation (28). The corresponding west face gradient is given by

$$\Delta x\left(\frac{\partial\Phi}{\partial x}\right)_w = \mathrm{GRADN} - \frac{c_x}{2}\,\mathrm{CURVN} - \frac{c_y}{2}\,\mathrm{TWIST} \tag{44}$$

The three-dimensional extensions of Equations (43) and (44) should, by now, be clear.

BENCHMARK TEST PROBLEMS

The well-known "rotating-velocity-field" convection problem is used as a benchmark test. The velocity field is that of solid-body rotation so that a given initial profile should be swept around as if it were imbedded in a rotating solid. For pure convection, the exact solution is thus known. The following three initial profiles are considered: a cylinder with a base diameter of 16 mesh-widths; a cone with the same base diameter; and a relatively narrow Gaussian distribution (σ = 2 mesh-widths). The computation is carried out on a 55 × 55 grid with a maximum Courant number near 0.8. Figure 6 shows results of the Lax-Wendroff simulation after one-half rotation in the counter-clockwise direction; the exact solutions have been juxtaposed, for reference. Note the typical trailing (phase-lag) oscillations, especially in the case of the cylinder. Figure 7 shows the corresponding two-dimensional second-order upwind simulation. In this case, phase-lead dispersion (partially obscured) occurs ahead of the simulated profile. Two nonoscillatory (TVD) schemes designed by Roe (reference 11) are shown in Figures 8 and 9. As seen, the Minmod results are quite diffusive for all profiles. Superbee does a reasonably good job on the cylinder, but tends to steepen and clip the other profiles. This is a well-known shortcoming of second-order-based TVD schemes, especially those of supercompressive type that rely on negative artificial diffusion to enhance discontinuity resolution; this is explained in detail in

reference 3. Finally, figure 10 shows results that can be obtained using methods described in this paper. The results shown are for a seventh-order upwind scheme including all third-order (but no higher) cross-terms. An *ad hoc* discriminator is used to relax limiter constraints in the vicinity of physical maxima; as mentioned before, an automatic multidimensional discriminator (similar to that described in reference 1 for one dimensional flow) is under development. This, of course, will be necessary before the code is applicable to general flow problems. Note from Figure 10 that resolution of the cylinder is better than that of Superbee, but without gross distortion of the other profiles.

CONCLUSION

The high-convection code described in this paper includes a number of features that are important for cost-effective accurate simulation of multidimensional unsteady flows on practical grids. Being based on third-order upwinding, the code is totally free of artificial numerical diffusion (or viscosity); this is important because schemes based on artificial-viscosity methods are often solving the wrong problem – i.e., an artificially *low*-convection problem rather than the physical *high*-convection problem. UTOPIA contains all necessary cross-terms to third order, thus matching all terms in the Taylor expansion of the complex amplitude ratio through to third order in the wave-number components. This guarantees excellent phase behaviour and isotropy regardless of the stream-to-grid angle. Codes based on second-order (or even fourth-order) *central* schemes inherently contain serious dispersion errors. Inclusion of the GRADT term should improve isotropy (in theory) – but this is usually masked by gross dispersion.

Although far more accurate than first- and second-order methods, third-order upwinding may give rise to slight overshoots or undershoots. This tendency can be eliminated by using the universal limiter, developed in reference 3, on each control-volume face, independently. If higher order resolution is required, the strategy of adaptive stencil expansion – increasing accuracy (above third order) only where needed – is extremely cost-effective. This is controlled by monitoring the absolute normal gradient and curvature across control-volume faces; as certain (pre-assigned) thresholds are exceeded, the code automatically switches to (in principle, arbitrarily) higher order accuracy at the face in question. Finally, in order to give full resolution to local extrema, the limiter constraints need to be automatically relaxed in such regions (in addition to using a higher order stencil). A fully automatic pattern-recognition discriminator of this type has been designed for one dimension (reference 1); the same principles appear to be applicable to multidimensional flows, as well, but a completely automatic multidimensional discriminator of this type is still under development.

REFERENCES

1. Leonard, B.P. and Niknafs, H.S., "Sharp Monotonic Resolution of Discontinuities Without Clipping of Narrow Extrema," *Computers and Fluids*, in press (1990).
2. Leonard, B.P., "A Stable and Accurate Convective Modelling Procedure Based on Quadratic Upstream Interpolation," *Computer Methods in Applied Mechanics and Engineering*, 19, 59-98 (1979).
3. Leonard, B.P., "Universal Limiter for Transient Interpolation Modeling of the Advective Transport Equations: The ULTIMATE Conservative Difference Scheme," NASA TM 100916 (ICOMP-88-11), NASA-Lewis Research Center.
4. Lax, P.D. and Wendroff, B., "Systems of Conservation Laws," *Communications on Pure and Applied Mathematics*, 13, 217-237 (1960).
5. Fromm, J.E., "A Method for Reducing Dispersion in Convective Difference Schemes," *Journal of Computational Physics*, 3, 176-189 (1968).
6. Leith, C.E., "Numerical Simulation of the Earth's Atmosphere," *Methods in Computational Physics*, 4, 1-28 (1965).

7. Warming, R.F. and Beam, R.M., "Upwind Second-Order Difference Schemes and Applications in Aerodynamic Flows," *AIAA Journal*, 14, 1241-1247 (1976).
8. Fletcher, C.A.J., *Computational Techniques for Fluid Dynamics*, Vols. I and II, Springer-Verlag, Berlin (1988).
9. Leonard, B.P., "Note on the von Neumann Stability of the Explicit FTCS Convective Diffusion Equation," *Applied Mathematical Modelling*, 4, 401-402 (1980).
10. Leonard, B.P., "Elliptic Systems: Finite Difference Method IV," in *Handbook of Numerical Heat Transfer*, (eds. W.J. Minkowicz, *et al.*), 347-378, Wiley, New York (1988).
11. Roe, P.L., "Characteristic-Based Schemes for the Euler Equations," *Annual Reviews of Fluid Mechanics*, 18 (eds. M. Van Dyke, *et al.*), Annual Reviews Inc. (1986).

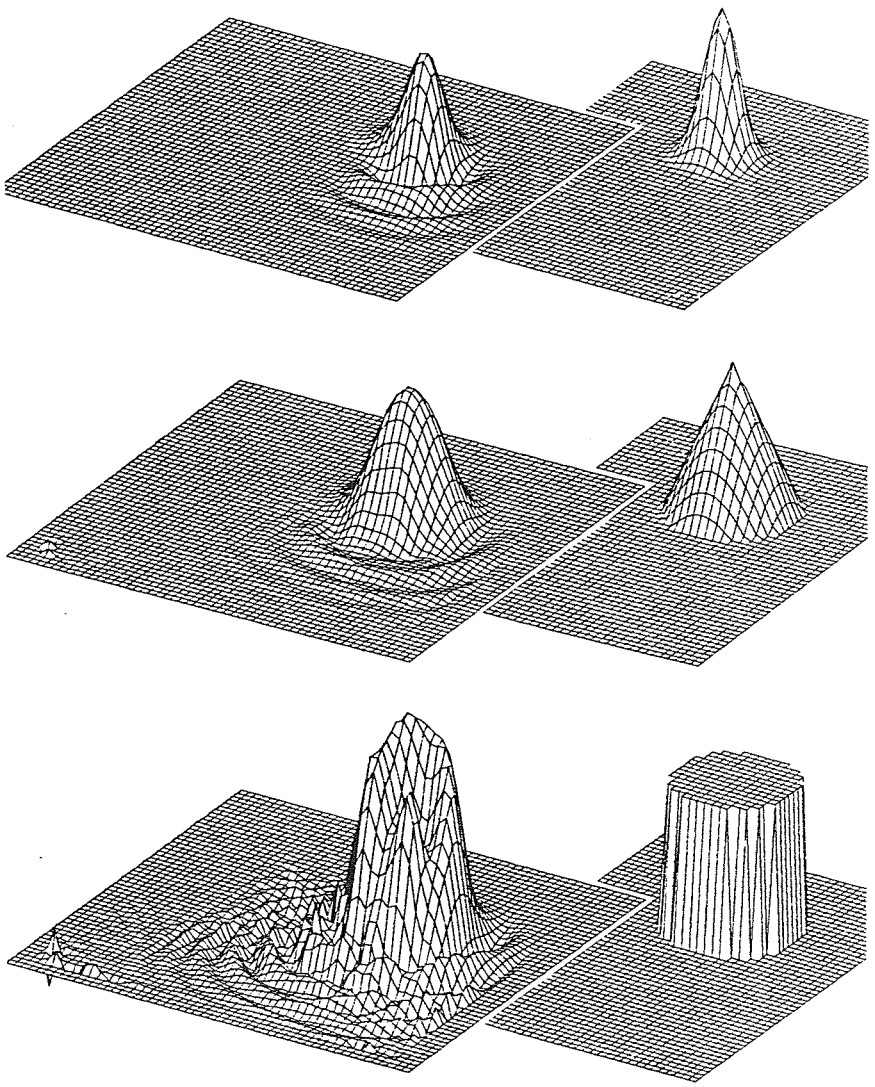

Figure 6. Lax-Wendroff simulation after one-half rotation counterclockwise compared with exact result.

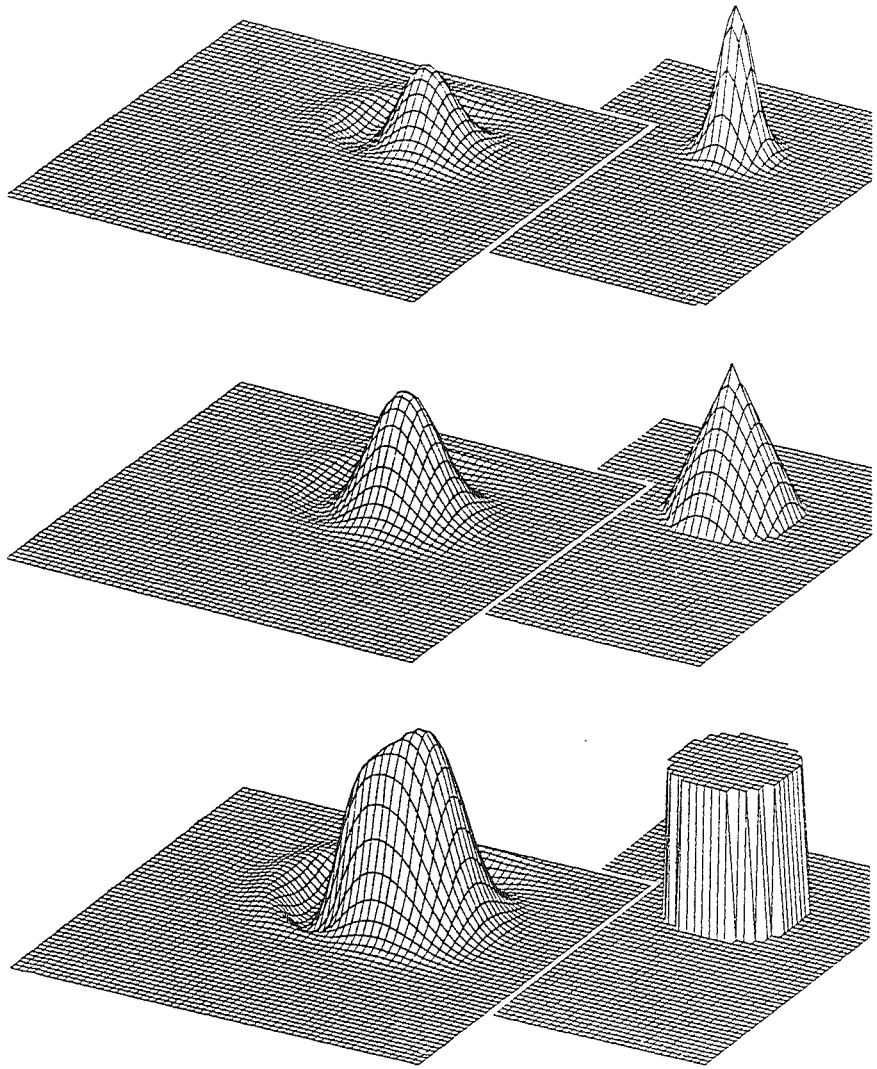

Figure 7. Second-order upwinding results after half rotation.

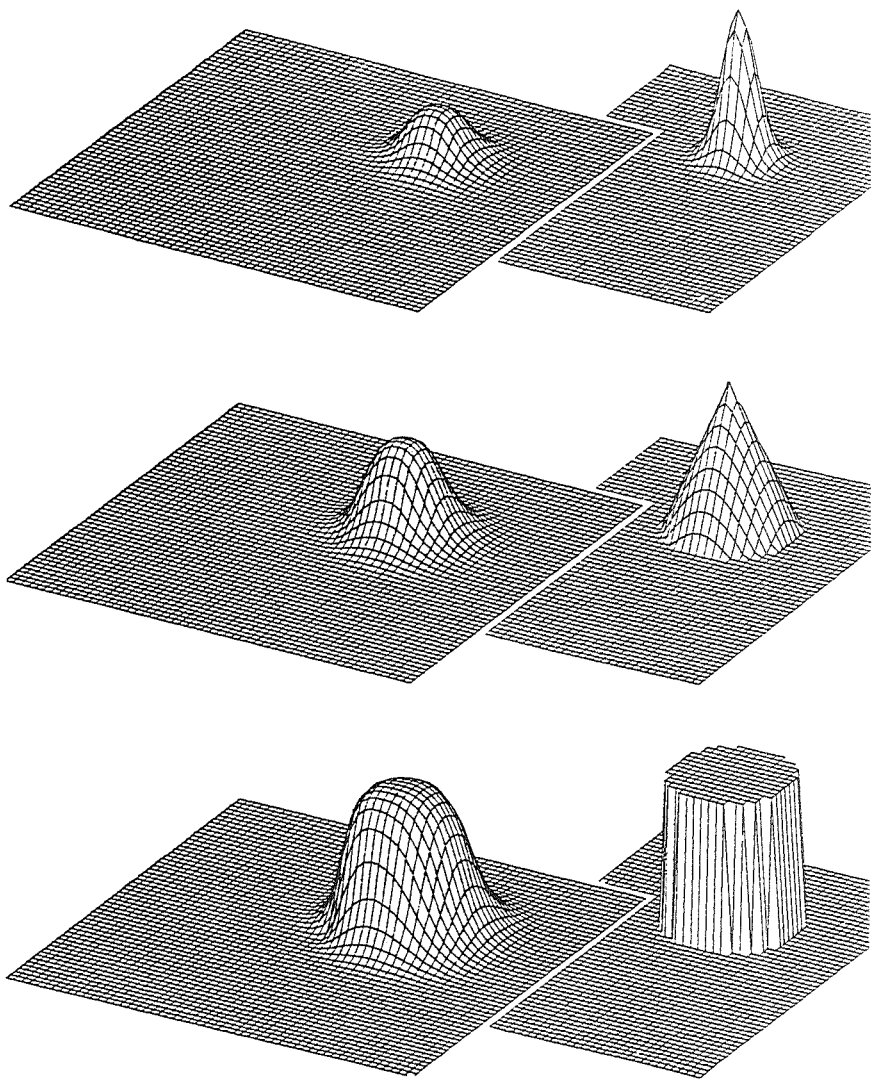

Figure 8. TVD-Minmod results.

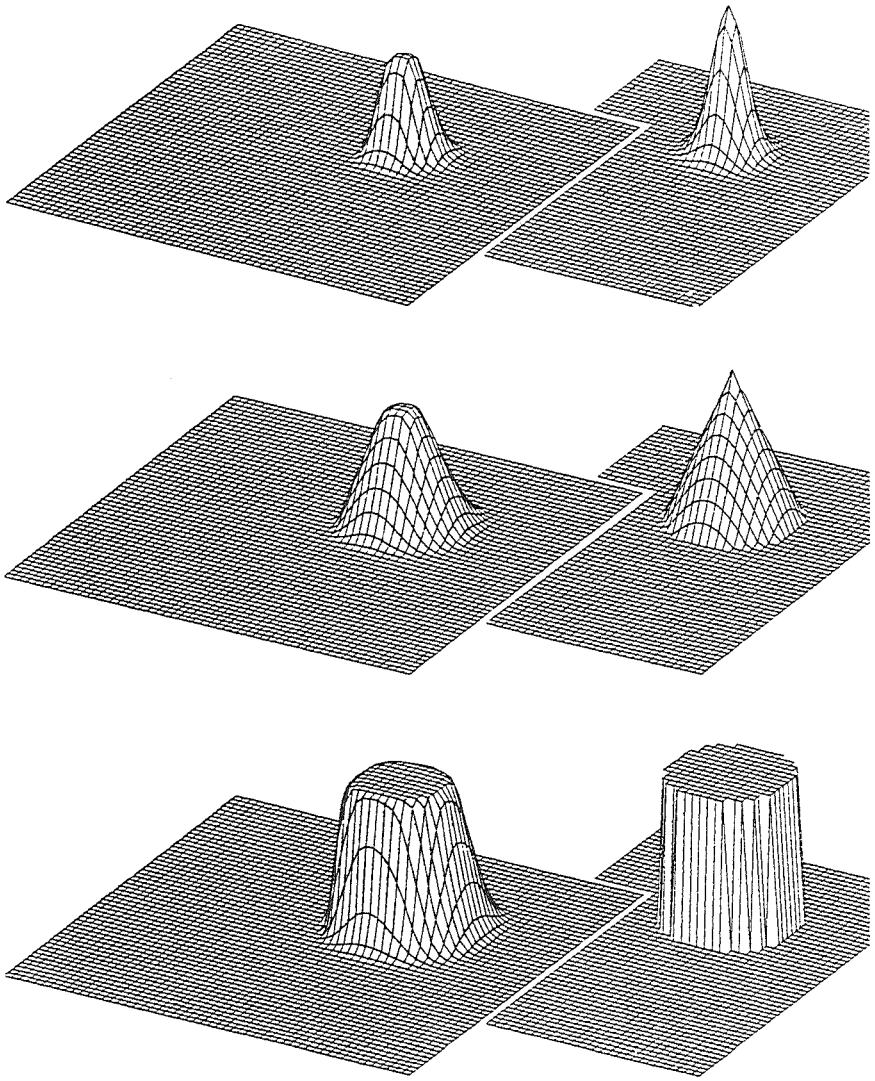

Figure 9. TVD-Superbee results.

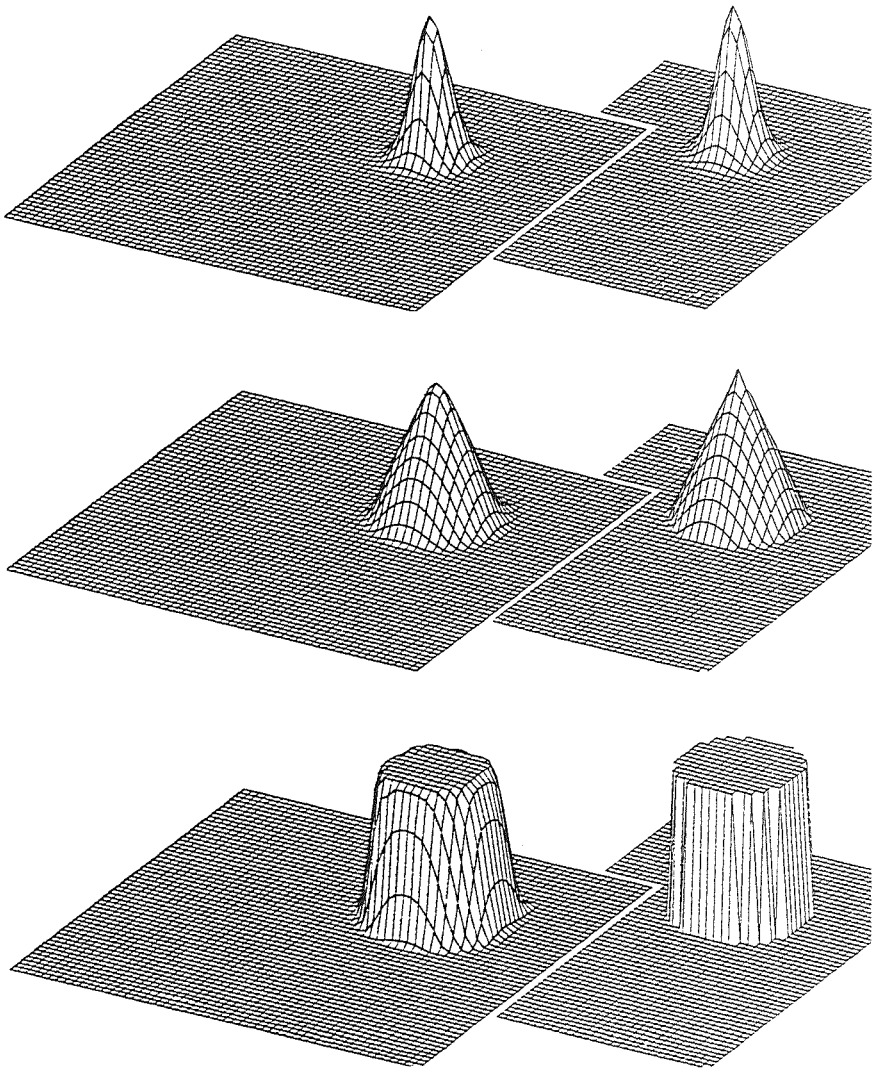

Figure 10. Results using the 3rd/7th-order method.